SHORT-TERM WIND FORCASTING AND ITS IMPACT ON THE MIX-MODE OPERATED BUILDINGS

Bing Dong[1] and Xiaoqian Jiang[2]
[1]United Technologies Research Center, East Hartford, CT, 06108, USA
[2]Division of Biomedical Informatics, University of California at San Diego, La Jolla, CA 92122

Abstract

In this paper, we developed a new method to forecast 10-minutes ahead wind speed based on Heteroscdastic Gaussian Process and investigated the impacts of this predicting on a mix-mode operated building. The forecasting result shows the mean absolute percentage error (MAPE) of 9.2%. The indoor air temperature, infiltration air change rate and cooling energy consumption varied 25% in average compared with the baseline model where the wind speed is not from forecasting.

Introduction

With the increasing use of energy in buildings, design and build energy efficient high performance buildings become more and more important. The best way for buildings to save on-site energy is to interact with its surrounding environment as much as possible. Natural and hybrid ventilation strategies have been widely implemented (Allard and Alvarez 1998; Heiselberg 2002; Lomas, Cook, and Fiala 2007). According to (Heiselberg 2002), a reduction of 20%~30% in overall energy consumption and 50% in electricity have been achieved comparing with full air conditioned office buildings. Most of the hybrid ventilation designs are based on simulation tools such as EnergyPlus, ESP-r or Computational Fluid Dynamics (CFD). Good et al.(Good, Frisque, and Phillips 2008) shows that not only the magnitudes of Cp values vary significantly for the different software, but also the predicting of the opening status can differ. Besides the different calculation methods could affect the decision of natural ventilation design, the wind speed data from different sources have very important impacts. The simulation of these software replies on historic data or real-time hourly data at most. However, the on-site wind speed can change dramatically within even one hour. Figure 1 shows the results of wind speed data from on-site measured 10 minutes interval and measured hourly data while interpolated by EnergyPlus into 10 minutes interval. The difference is up to ±35% of measured 10 minutes data. Unfortunately, most of the weather forecasting websites will not provide 10 minutes ahead wind speed forecasting, but only hourly. This phenomena motivates to the purpose of this study: 1) develop a new method to forecast 10 minutes ahead wind speed; 2) investigate the impacts of such forecasting on the building cooling energy consumption and indoor environment based on a small-scale mix-mode operated building setup in EnergyPlus, where airflow network model is used to simulate building natural ventilation.

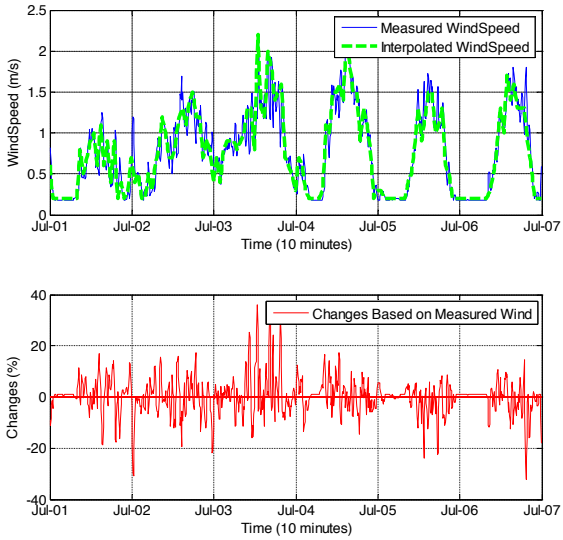

Figure 1: Comparison of 10 minutes wind speed from two different resources

Methodology

Various time series regression approaches have been applied to the problem of short term wind speed forecast. Steftsos (Steftsos 2000) applied various data mining techniques to forecast mean hourly wind speed . These techniques include linear models (ARMA), feed forward and recurrent neural networks (NNT), adaptive neuro-fuzzy inference systems and neural logic networks. The results show that NNT methods are better than other linear and non-linear models within 5% in terms of root mean square error (RMSE). Most recently, Palomares-Salas et al. (Salas et al. 2009) compared two models, ARMA and NNT, for short term wind speed forecasting (10 minutes, 1 hour, 2 hours and 4 hours) and the results are very similar with average RMSE from 0.57 to 1.55.

Alternatively, as the wind speed has momentum over time,

it can be treated as transitional behavior and modeled as a Markov Process. Tore et al. (Tore, Poggi, and Louche 2001) used first order Markov chain models for synthetic generation of hourly wind speed time series in Turkey. Youcef et al. (Youcef, H., and A. 2003) modeled both hourly wind speed and wind direction data based on Markov chains. Shamshad et al. (Shamshad et al. 2005) have generated hourly wind speed data using first and second order Markov chains and compared the first and second order Markov chains using wind speed data measured from two different regions in Malaysia . In their study, it was concluded that the wind speed behavior slightly improves at the increasing order of the Markov model.

In the literature, very few studies focused on a short-time (10 minutes) forecasting. In this paper, we present a novel method called Heteroscedastic Gaussian Process (HGP) to tackle the short term wind speed forecasting problem. Gaussian process (GP), unlike other regression techniques, is defined as a distribution over functions, and inference takes place directly in the space of functions. The model combines a loss function with the predictive distribution using decision theory to make point distributions in an optimal way. Please refer to section NOMENCLATURE for notation details.

Gaussian process formulation

A Gaussian process is completely specified by its mean function and covariance function. We define the mean function $m(X)$ and the covariance function $k(X,X')$ of a real process $h(X)$ as

$$m(X) = E[h(X)], \quad (1)$$
$$k(X,X') = E[(h(X)-m(X))(h(X')-m(X'))], \quad (2)$$

and will write the Gaussian process as

$$h(X) \sim gp(m(X),k(X,X')). \quad (3)$$

The random variables represent the value of the function $h(X_t)$ over time, i.e. where the index set t of the random variable X_t is time. One of the most important properties of GP is known as the marginalization property. This simply means that if the GP e.g. specifies $(Y_1,Y_2) \sim N(\mu,\Sigma)$, then it must also specify $Y_1 \sim N(\mu_1,\Sigma_{11})$, where Σ_{11} is the relevant sub-matrix of Σ. In other words, examination of a larger set of variables does not change the distribution of the smaller set.

In function space, a simple example of Gaussian process can be obtained from a Bayesian linear regression model $h(X) = \phi(\mathbf{X})^T\mathbf{w}$, with a prior $\mathbf{w} \sim N(0,\Sigma_p)$, feature function $\phi(\mathbf{X})$. The mean and variance of $h(X)$ is,

$$E[h(X)] = \phi(X)^T E[\mathbf{w}] = 0, \quad (4)$$

$$E[h(X)h(X')] = \phi(X)^T E[\mathbf{w}\mathbf{w}^T]\phi(X') = \phi(X)^T\Sigma_p\phi(X'), \quad (5)$$

where $h(X)$ and $h(X')$ are joint Gaussian with zero mean and covariance given by $\phi(X)^T\Sigma_p\phi(X')$. Note N represents the feature vector length of X while T represents the length of the time series. If $N < T$ then this Gaussian is singular (as the joint covariance matrix will be of rank N).

A common choice of covariance function is the squared error covariance function, which specifies the covariance between pairs of random variables,

$$cov(h(X),h(X')) = k(X,X') = \exp(-\frac{1}{2}|X-X'|^2/l), \quad (6)$$

where the positive constant l changes the characteristic length-scale of the process. The covariance is almost unity between variables whose corresponding inputs are very close, and decreases quickly as their distance in the input space decreases. This specification of covariance function implies a distribution of functions.

Forecasting with noise-free observations

The previous section discussed about the training procedure of GP but we are most interested in forecasting future observations. Let's first consider simple cases where the observations are noise free, that is we know $\{(X_t,h_t)|t = 1,\ldots,T\}$. The joint distribution of the training outputs, $\mathbf{f}$, and the test output $\mathbf{f}_*$ according to the prior is

$$\begin{bmatrix} \mathbf{h} \\ \mathbf{h}_* \end{bmatrix} \sim N(0, \begin{bmatrix} K(\mathbf{X},\mathbf{X}) & K(\mathbf{X},X_*) \\ K(X_*,\mathbf{X}) & K(X_*,X_*) \end{bmatrix}). \quad (7)$$

If there are T training points and T_* test points then $K(\mathbf{X},X_*)$ denotes the $T \times T_*$ matrix of the covariance evaluated at all pairs training and test points, and similarly for all other entries. To get the posterior distribution over functions we need to restrict this joint prior distribution to contain only those functions which agree with the observed data points. Fortunately, in probabilistic terms this is very simple, corresponding to conditioning the joint Gaussian prior distribution on the observation to give

$$\mathbf{h}_*|X_*,\mathbf{X},\mathbf{h} \sim N(K(X_*,\mathbf{X})K(\mathbf{X},\mathbf{X})^{-1}\mathbf{f}), \quad (8)$$
$$K(X_*,X_*) - K(X_*,\mathbf{X})K(\mathbf{X},\mathbf{X})^{-1}K(\mathbf{X},X_*)).$$

Function values $\mathbf{h}_*$ can be sampled from the joint posterior distribution by evaluating the mean and covariance matrix from the above function and generating samples.

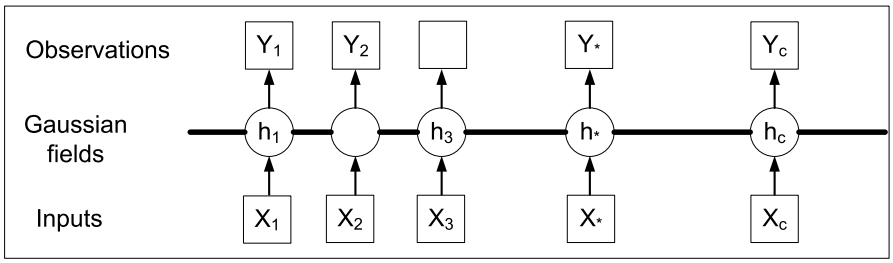

Figure 2: Graphical model for a GP regression model. X_t Y_t represent observed variables and h_t represents unknowns. The thick horizontal bar represents a set of fully connected nodes over time.

Forecasting with homogeneous noisy observations

In more realistic modeling, we often do not have access to function values themselves, but only noisy versions thereof $Y = h(X) + \varepsilon$. Assuming additive independent identically distributed Gaussian noise ε with homogeneous variance σ^2, the prior on the noisy observation becomes

$$cov(Y,Y') = k(X,X') + \sigma^2 \delta_{xx'}, \tag{9}$$

where $\delta_{xx'}$ is a delta function which is one if and only if the index of x is identical to x' and zero otherwise. Introducing the noise term, we can write the joint distribution of the observed target values and the function values at the test location under the prior as

$$\begin{bmatrix} \mathbf{Y} \\ \mathbf{h}_* \end{bmatrix} \sim N(0, \begin{bmatrix} K(\mathbf{X},\mathbf{X}) + \sigma_t^2 I & K(\mathbf{X},X_*) \\ K(X_*,\mathbf{X}) & K(X_*,X_*) \end{bmatrix}). \tag{10}$$

Deriving the conditional distribution, we arrive at the key forecasting equations for Gaussian process regression,

$$\mathbf{h}_*|X_*,\mathbf{X},\mathbf{Y} \sim N(\bar{\mathbf{h}}_*, cov(\mathbf{h}_*)), \tag{11}$$

$$\bar{\mathbf{h}}_* = E[\mathbf{h}_*|X_*,X,Y] = K(X_*,\mathbf{X})[K(\mathbf{X},\mathbf{X}) + \sigma^2 I]^{-1}\mathbf{Y}, \tag{12}$$

$$cov = K(X_*,X_*) - K(X_*,\mathbf{X})[K(\mathbf{X},\mathbf{X}) + \sigma^2 I]^{-1}K(\mathbf{X},X_*). \tag{13}$$

For any set of basis functions, we can compute the corresponding covariance function as $k(x,x') = \phi(x)^T \Sigma_p \phi(x')$. We can rewrite the functions above to make it uncluttered. Let $K = K(\mathbf{X},\mathbf{X})$ and $K_* = K(\mathbf{X},X_*)$ and denote $k(X_*) = k_*$as the vector of covariance between the test point and the T training points, we reduce the original functions to

$$\begin{aligned} \bar{\mathbf{h}}_* &= k_*^T[K + \sigma^2 I]^{-1}\mathbf{Y}, & (14) \\ cov(\mathbf{h}_*) &= K(X_*,X_*) - k_*^T[K + \sigma^2 I]]k_*. & (15) \end{aligned}$$

One way to look at the prediction function $\bar{\mathbf{f}}_*$ is to see it as a linear combination of kernel functions, each one centered on a training point, by writing $\bar{\mathbf{h}}_* = \sum_{t=1}^{T} \alpha_i k(X_i,X_*)$, where $\alpha = (K + \sigma_t^2 I)^{-1}Y$, reveals the fact that the GP can be represented in terms of a number of basis function. Intuitively, we can understand the result because although GP defines a joint Gaussian distribution over all the y variables, one for each point in the index set $\mathcal{X}$ in making prediction at x_*, we only care about the $(n+1)$-dimensional distribution defined by the n training points and the test point.

Forecasting with heteroscdastic noisy observations

To deal with more complicated nature environments, e.g. wind speed, we need to relax our assumptions. To this end, we model the noise by a function of X, thus we get a Heteroscdastic regression problem, where the noise rate is not assumed constant on the domain. By placing a Gaussian process prior on h and assuming a noise rate function $r(x)$, the predictive distribution $P(\mathbf{h}_*|X_*,X,Y)$ at the query points X_* is a multivariate Gaussian distribution

$$\begin{aligned} \mathbf{h}_*|X_*,\mathbf{X},\mathbf{Y} &\sim N(\bar{\mathbf{h}}_*, cov(\mathbf{h}_*)), & (16) \\ \bar{\mathbf{h}}_* &= k_*^T[K + Z]^{-1}\mathbf{Y}, & (17) \\ cov(\mathbf{h}_*) &= K(X_*,X_*) - Z_* - k_*^T[K + Z]]k_*, & (18) \end{aligned}$$

where $Z = diag(\mathbf{z})$ with $\mathbf{z} = (z(X_1),\ldots,z(X_T))^T$ and $Z_* = diag(\mathbf{z}_*)$ with $\mathbf{z}^* = (z_*(X_1),\ldots,z_*(X_T))^T$.

We use an independent GP to model the noise levels, this z-process is governed by a different covariance function k_z, parameterized by θ_z. The locations $X_1,\ldots,X_n$ of the training data points $Z = \{z_1,\ldots,z_n\}$for the z-process can be chosen arbitrarily, however, for notational convenience, we set them to coincide with the ones of the t-process here.

Since the noise rates z_i are independent latent variables in the combined regression model, the predictive distribution for $\mathbf{h}_*$, the vector of regressands at points $X_*$is,

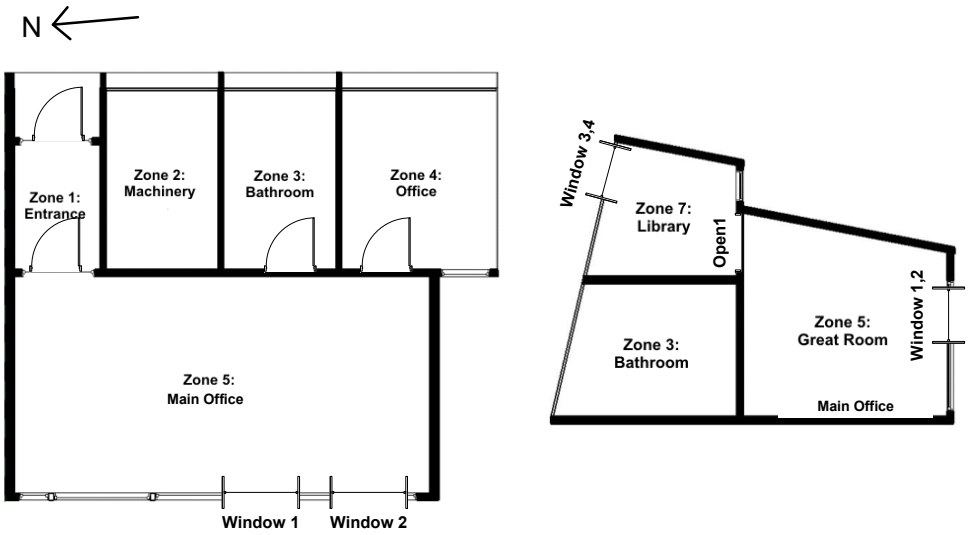

Figure 3: Plan and section views of the test building

$$P(\mathbf{h}_*|X_*,\mathbf{X},\mathbf{Y}) = \int\int P(\mathbf{h}_*|X_*,\mathbf{X},\mathbf{Y},\mathbf{Z},Z_*)P(\mathbf{Z},Z_*|X_*,\mathbf{X},\mathbf{Y})d\mathbf{Z}dZ_*.$$

Given $(\mathbf{Z},Z_*)$, the predictive process is Gaussian with specified mean and variance. The real problematic term is thus $P(\mathbf{Z},Z_*|X_*,\mathbf{X},\mathbf{Y})$ as it makes the integral difficult to handle analytically. (Goldberg, Williams, and Bishop 1998) and (Le, Smola, and Canu 2005) suggested Monte Carlo approximation and full Bayesian treatment, respectively. But both computation is quite time consuming. A recent paper (Kristian et al. 2007) suggested an iterative procedure to estimate the most likely per sample noise and showed good empirical performance.

We suggest an easy way to estimate with the two rounds of optimizations. First, we assume a homogeneous Gaussian noise ε with variance σ^2 to learn an ordinary Gaussian Process $\hat{h}$ with kernel K_o. Then, we estimate the covariance from $\dot{\mathbf{X}} = \mathbf{X} \cup X_*$. Next, we plugin the covariance error of $\dot{\mathbf{X}}$ to form the new kernel.

$$K_n = K_o - \sigma^2 I_N + \sigma^2_{\hat{h}}(\dot{\mathbf{X}})I_N. \tag{19}$$

Finally the value of the future wind speed X_* is estimated as the mean of the posterior

$$\tilde{X}_* = k_T'(\hat{K}_n + \sigma^2 I)^{-1}\mathbf{X}, \tag{20}$$

where $\hat{K}_n$ is composed of the rows and columns of K_n corresponding to $\mathbf{X}$. We can add an small noise variance σ^2 to our new function h to give robustness to the inversion of $\hat{K}_n$.

We suggest a different way to approximate the expectation by the most likely noise levels $(\tilde{\mathbf{Z}},\tilde{Z}_*)$, that is we approximate the predictive distribution by $P(\mathbf{h}_*|X_*,\mathbf{X},\mathbf{Y}) \approx P(\mathbf{h}_*|X_*,\mathbf{X},\mathbf{Y},\tilde{\mathbf{Z}},\tilde{Z}_*)$, where $(\tilde{\mathbf{Z}},\tilde{Z}_*) = argmax_{(\tilde{\mathbf{Z}},\tilde{Z}_*)}P(\tilde{\mathbf{Z}},\tilde{Z}_*|X_*,\mathbf{X},\mathbf{Y})$. This will be a good approximate if most of the probability mass of $P(\mathbf{Z},Z_*|X_*,\mathbf{X},\mathbf{Y})$ is concentrated around $(\tilde{\mathbf{Z}},\tilde{Z}_*)$. Moreover, computing the most likely noise level and $P(\mathbf{h}_*|X_*,\mathbf{X},\mathbf{Y})$ now requires only standard GP inference, much faster than sampling approaches.

Evaluating

The model efficacy is evaluated in Root Mean Square Error (RMSE) and Mean Absolute Percentage Error (MAPE).

$$\text{MAPE} = \frac{1}{n}\sum_{t=1}^{n}\left|\frac{A_t - F_t}{A_t}\right| \tag{21}$$

$$\text{RMSE} = \sqrt{\frac{1}{n}\sum_{t=1}^{n}(A_t - F_t)^2}, \tag{22}$$

parameterized where A_t is the actual value and $F_t$is the forecast value.

Experiment setup

Wind speed forecasting

The wind speed sensor was installed two feet above the highest point of the experiment building. It measures the

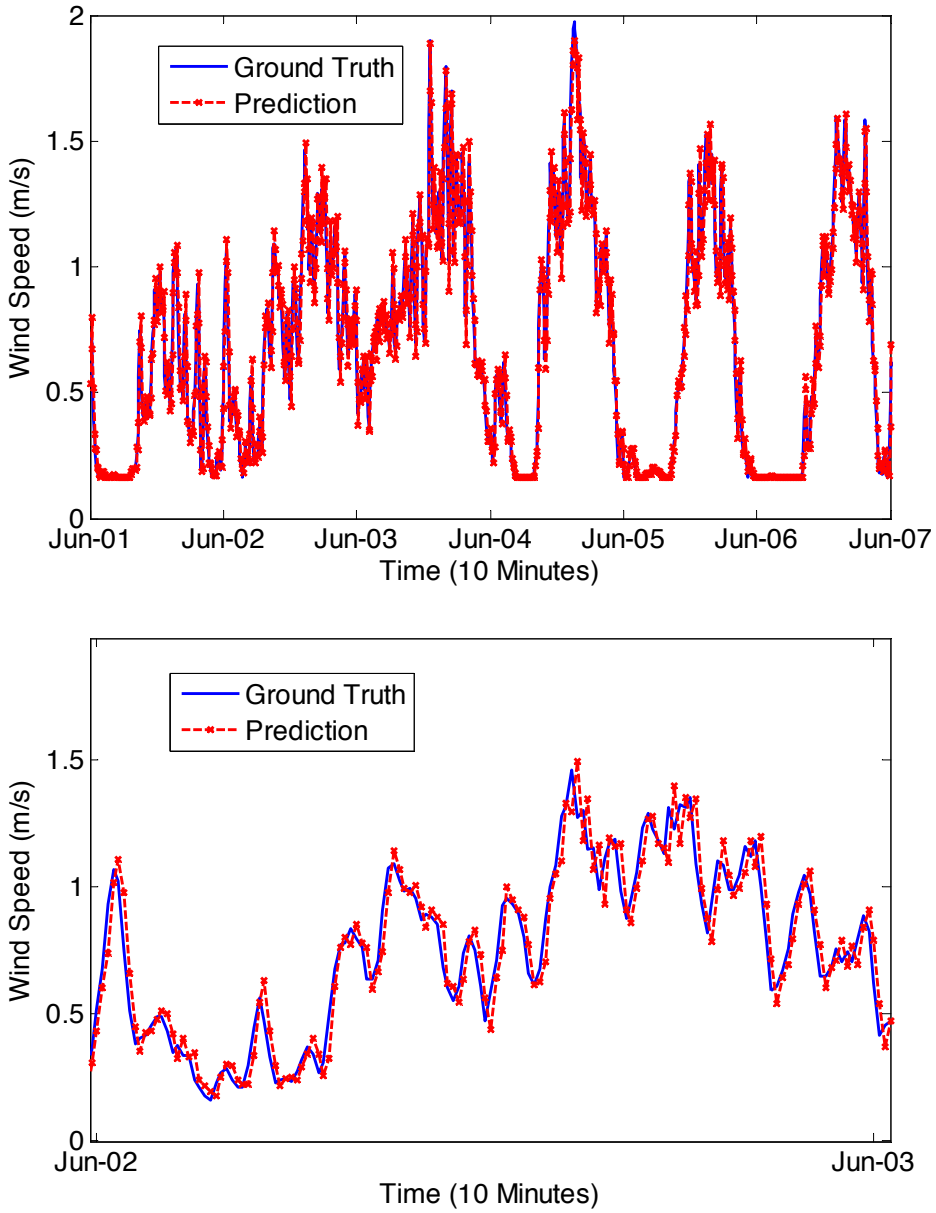

Figure 4: Results of wind speed forecasting.

wind speed every five seconds and is stored into a database every one minute. The data is continuously collected since April, 2009. In this study, the data from June 1st to 30th, 2009 was used for training and from July 1st to 6th was used for testing.

Simulating of a mix-mode operated building

A mix-mode operated building on campus was used as the simulation testbed. It is a two story small building with two offices and is used as an office building. Figure 3 shows the overall geometry of the building. There are two windows in the great room, three windows in the upper space of the office (a double volume space) and three back windows in the library are openable. Office and great room are connected by doors in the lower level and holes in the upper level.

The air flow through windows and doors were simulated based on EnergyPlus Airflow Network, with natural ventilation set-point of 18 C. In addition, only great room and office are equipped with a cooling system with indoor air temperature set point of 24 C. The hybrid ventilation control is based on temperature and wind speed with maxi-

mum outside wind speed of 5 m/s and outside temperature of 22 C. The night setback is 28 C from 6:00pm to the next day 8:00am.

The simulation period is from July 1st to July 6th, when natural ventilation is possible most of the time. One of the main purposes in this study is to compare the effects of two different wind speeds only. Hence, during the EnergyPlus simulation, all other inputs in the weather file are the same except the wind speed. In addition, the outdoor dry-bulb air temperature and wind direction in the weather file were also from on-site continuous measured data.

Results and discussion

Table 1: List of results of different methods from 10-minutes ahead forecasting

Model	MAPE	RMSE	Variance(%)
HGP	9.2	0.0092	0.8
ARMA	12.3	0.13	1.7
SVR	9.8	0.1	1.1
ANN	25	0.21	4.6

Wind speed

Figure 4 shows the results of ten minutes ahead forecasting of on-site real time wind speed using HGP. The RMSE is 0.092 with variance 0.008594. In addition, other recently used methods were also run on the same datasets and compared with HGP. The other methods are Support Vector Regression (SVR), Artificial Neural Network (ANN) and Autoregressive Moving Average (ARMA). The results are listed in Table 1. HGP has the best result while ANN has the worst one in terms of RMSE. The ANN used in this study has three layers with 10 nodes and sigmoid function on the hidden layer. Among all other methods, only HGP considers the dynamic changes of noise term. SVR method has the similar result with HGP, which maps the input and output data into a high dimension space and correlates them but it does not handle Heteroscedastic noise.

Cooling energy

The forecasting result from the wind speed is used as an input into the mix-mode simulation in EnergyPlus (DOE 2009). Another wind speed source is from the hourly measured data while interpolated by EnergyPlus into 10 minutes. The cooling energy usages are shown in Figure 5 above. It shows that at different time periods, the cooling energy consumption varies because of different wind speed within a short-time period. For example, on the day of July 1st , the cooling energy from wind-speed-1 (measured) happened more frequently than wind-speed-2 (EnergyPlus interpolated). However, on July 3rd, there is no

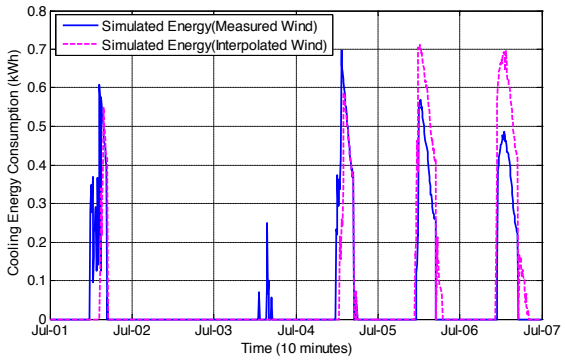

Figure 5: Cooling energy consumption from two different wind speed sources

cooling needed from wind-speed-2. In addition, on July 5th and 6th, cooling energy from wind-speed-1 is less than the one from wind-speed-2. Overall, the total cooling energy consumption from wind-speed-1 and wind-speed-2 are 94kWh and 99kWh, respectively. In order to investigate the insights, indoor air temperature and air change rate were analyzed in the next section.

Indoor environment

July 1st and 5th were picked up for detailed analysis. Figure 6 (a) shows the simulated indoor and measured outdoor temperature on July 1st in the great room. The simulated indoor mean air temperature from two different wind speed sources vary slightly different (within 1 C) during the noon time. Figure 6 (b) shows the zone infiltration air change rate (ACH), July 1st and 5th were picked up for detailed analysis. Figure 6 (a) shows the simulated indoor and measured outdoor temperature on July 1st in the great room. The simulated indoor mean air temperature from two different wind speed sources vary slightly different (within 1 C) during the noon time. Figure 6 (b) shows the zone infiltration air change rate (ACH), which represents the number of air changes per hour produced by outdoor air flow into the zone from window/door openings and cracks in the exterior surfaces of the zone (DOE, 2009). Overall, the cooling happened at different time of the day for these two wind speeds. The cooling energy needs from wind-speed-1 is higher than the one from wind-speed-2. In addition, the infiltration air change rate from wind-speed-2 is up to 46% higher than wind-speed-1, especially during the day time. This is because outside wind-speed-2 is larger than wind-speed-1 on July 1st as shown in Figure 1which represents the number of air changes per hour produced by outdoor air flow into the zone from window/door openings and cracks in the exterior surfaces of the zone. Overall, the cooling happened at different time of the day for these two wind speeds. In ad-

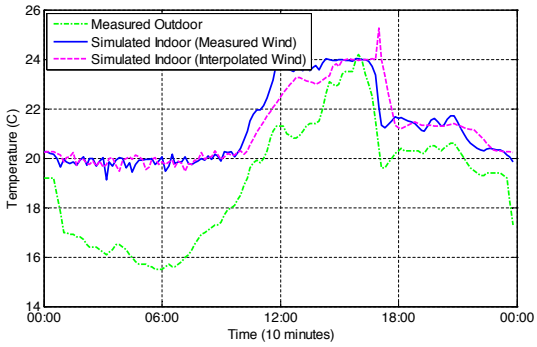

(a)

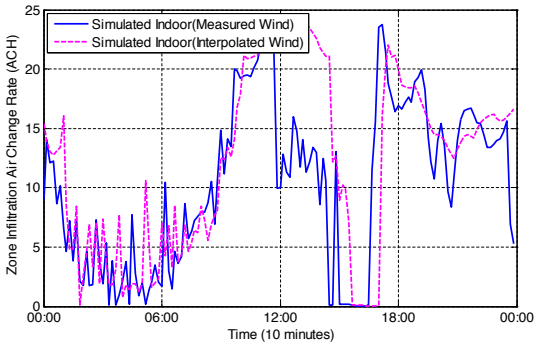

(b)

Figure 6: (a),air temperature on July 1st (b) zone infiltration air change rate on July 1st.

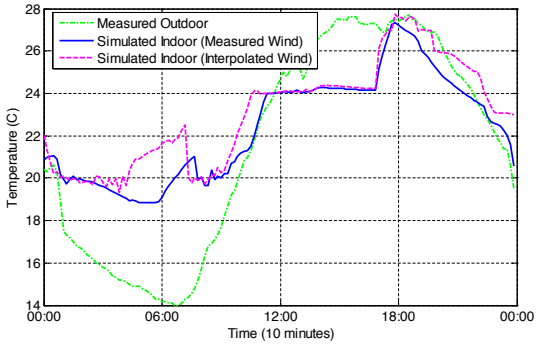

(a)

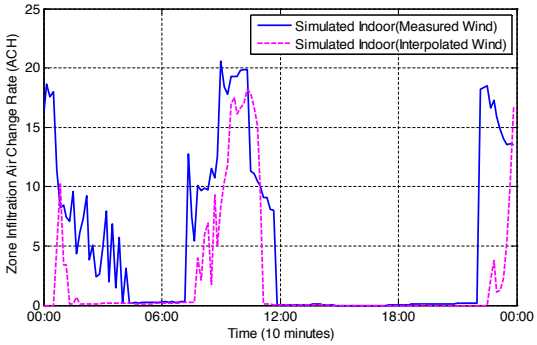

(b)

Figure 7: (a) Air temperature on July 5th (b) Zone infiltration air change rate on July 5th.

dition, the infiltration air change rate from wind-speed-2 is up to 46% higher than wind-speed-1, especially during the day time. This is because outside wind-speed-2 is larger than wind-speed-1 on July 1st as shown in Figure 1. The natural ventilation time from wind-speed-2 is also longer. This explains the cooling energy needed by wind-speed-1 is more.

Figure 7 (a) and (b) shows the air temperature and the zone infiltration air change rate on July 5th, when the cooling needs from wind-speed-2 is more than wind-speed-1. The indoor air temperature around 6:00am from wind-speed-2 is higher than that from wind-speed-1 because infiltration air change rate from wind-speed-1 at night is 20% higher in average. This is also illustrated in Figure 1, where the wind-speed-1 is higher than wind-speed-2 at night. This also causes the zone air temperature from wind-speed-2 is a bit higher than wind-speed-1 before the cooling on around 11:00am, which leads to the higher cooling energy use for wind-speed-2.

Sensitivity analysis

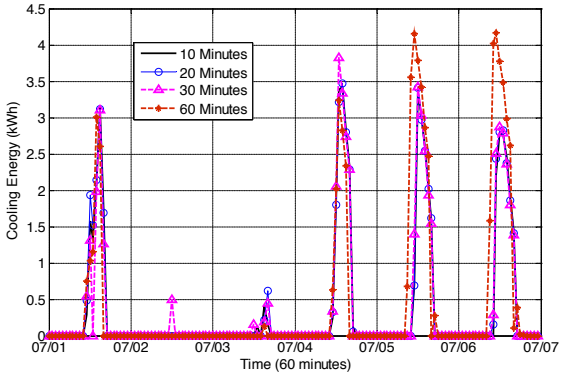

Figure 8: Comparison of cooling energy consumption from four different frequencies of measured wind speed

After all the simulation tests, we found that the indoor environment and energy consumption could vary according to different wind speed resources. In this section, we

will discuss whether the frequencies of wind speed inputs based on the same data source would impact. The on-site measured wind speed data from 10 minutes, 20 minutes, 30 minutes and 60 minutes intervals were used as inputs into the mix-mode operated building model. Figure 8 shows the results of hourly cooling energy consumption from these inputs. Overall, different frequencies of wind speed have different cooling energy consumption patterns, particularly in natural ventilation dominated days such as July 1st to July 3rd. On cooling energy dominated days, the more frequent of the wind speed, the less the cooling energy consumption, but very slightly. The 60 minutes interval wind speed data have larger impacts on the cooling energy than others.

Conclusion

In this paper, we presented a new method to forecast the short-term wind speed. This new method performs 20% better in average than other recently used methods in terms of prediction accuracy. In addition, the forecasting results were used as inputs into a simulation of a mix-mode operated building. The energy and indoor environment performance were compared with the wind speed interpolated by EnergyPlus. The results show that although cooling energy consumption from two sources differs slightly, the total cooling energy consumption pattern varies significantly due to the different zone infiltration air change rate. The future study will focus on applying this wind forecasting method into model predictive control in natural ventilation buildings.

Nomenclature

$\mathbf{X} = [X_1, \ldots, X_T]'_{T\times 1}$	Feature vector
$\mathbf{Y} = [Y_1, \ldots, Y_T]'_{T\times 1}$	Target values
$m(X)$	Mean function
$k(X, X')$	Covariance function
$f(X)$	GP function
$\mathbf{h}=\{h_1, \ldots, h_t, \ldots, h_T\}$	Random variable corresponds to the case $(X_t, Y_t)\|_{t=1}^{T}$
$\phi(\mathbf{X})^T$	Feature function for $\mathbf{X}$
$\mathbf{w}$	Weight vector
$k(X, X') = \exp(-\frac{1}{2}\|X - X'\|^2)$	Kernel function
$K = K(\mathbf{X}, \mathbf{X})$, $K_* = K(\mathbf{X}, X_*)$, $k(X_*) = k_*$	Kernel matrix
$N = \|\phi(\mathbf{X})^T\|$	Length of the feature

References

Allard, F. S., and M. S. Alvarez. 1998. "European Commission." *Directorate-General for Energy, ALTENER Programme. Natural ventilation.*

DOE. 2009. "EnergyPlus V4.0 Input-output Reference."

Goldberg, Paul W., Christopher K. I. Williams, and Christopher M. Bishop. 1998. "Regression with input-dependent noise: a Gaussian process treatment." *NIPS 97: Proceedings of the 1997 conference on Advances in neural information processing systems.*, pp. 493–499.

Good, J., A. Frisque, and D. Phillips. 2008. "The role of Wind in Natural Ventilation Simulations Using Airflow Network Models." *Proceedings of SimBuild 2008* 30:693šC708.

Heiselberg, P. 2002. *Principles of hybrid ventilation*. Aalborg University, Aalborg, Denmark.

Kristian, K., Plagemann C., Pfaff P., and Burgard W. 2007. "Most likely Heteroscedastic Gaussian process regression." *ICML 07: Proceedings of the 24nd international conference on Machine learning.*, pp. 393–400.

Le, Q. V., A. J. Smola, and S. Canu. 2005. "Heteroscedastic Gaussian process regression." *ICML 05: Proceedings of the 22nd international conference on Machine learning.*, pp. 489–496.

Lomas, k.J., M.J. Cook, and D. Fiala. 2007. "Low energy architecture for a server US climate: design and evaluation of a hybrid ventilation strategy." *Energy and Buildings* 29:32–44.

Salas, J.C. Palomares, J.J. G. Rosa, J.G. Ramiro, J.Melgar, A. Aguera, and A. Moreno. 2009. "Comparison of Models for Wind Speed Forecasting." Proc. of International Conference on Computational Science.

Shamshad, A., M. A. Bawadi, Hussin W. W., T. A. Majid, and S. Sanusi. 2005. "First and second order markov chain models for synthetic generation of wind speed time series." *Energy* 30:693–708.

Steftsos, S. 2000. "A comparison of various forecasting techniques applied to mean hourly wind speed time series." *Renew Energy* 21:23–35.

Tore, M.C., P. Poggi, and A. Louche. 2001. "Markovian model for studying wind speed time series in corsica." *Renew Energy* 3:311šC319.

Youcef, F., Sauvageot H., and Adane A. 2003. "Statistical bivariate modeling of wind using first order markov chain and weibull distribution." *Wind Engineering* 28:87šC80.